Received: 7 August 2022 | Revised: 25 October 2022 | Accepted: 26 October 2022

DOI: 10.1002/stc.3144

RESEARCH ARTICLE

WILEY

Gross outlier removal and fault data recovery for SHM data of dynamic responses by an annihilating filter-based Hankel-structured robust PCA method

Si-Yi Chen[1,2] | **You-Wu Wang**[1,2] | **Yi-Qing Ni**[1,2]

[1]Department of Civil and Environmental Engineering, The Hong Kong Polytechnic University, Hung Hom, Kowloon, Hong Kong S.A.R.

[2]National Rail Transit Electrification and Automation Engineering Technology Research Center (Hong Kong Branch), The Hong Kong Polytechnic University, Kowloon, Hung Hom, Hong Kong S.A.R.

Correspondence
Y.Q. Ni, National Rail Transit Electrification and Automation Engineering Technology Research Center (Hong Kong Branch), The Hong Kong Polytechnic University, Hung Hom, Kowloon, Hong Kong S.A.R.
Email: ceyqni@polyu.edu.hk

Funding information
Research Grants Council of the Hong Kong Special Administrative Region, China, Grant/Award Number: PolyU 152014/18E; National Natural Science Foundation of China, Grant/Award Number: U1934209; Innovation and Technology Commission of Hong Kong SAR Government, Grant/Award Number: K-BBY1

Abstract

In daily monitoring of structures instrumented with long-term structural health monitoring (SHM) systems, the acquired data is often corrupted with gross outliers due to hardware imperfection and/or electromagnetic interference. These unexpected spikes in data are not unusual and their existence may greatly influence the results of structural health evaluation and lead to false alarms. Hence, there is a high demand for executing data cleaning and data recovery, especially in harsh monitoring environment. In this paper, we propose a robust gross outlier removal method, termed Hankel-structured robust principal component analysis (HRPCA), to remove gross outliers in the monitoring data of structural dynamic responses. Different from the deep-learning-based approaches that possess only outlier identification or anomaly classification ability, HRPCA is a rapid and integrated methodology for data cleaning, which enables outlier detection, outlier identification, and recovery of fault data. It capitalizes on the fundamental duality between the sparsity of the signal and the rank of the structured matrix. Using annihilating filter-based fundamental duality, structural responses could be modeled as lying in a low-dimensional subspace with additional Hankel structure; thus, the gross outliers could be represented as a sparse component. Then the outlier removal issue turns into a matrix factorization problem, which could be successfully solved by robust principal component analysis (RPCA). To validate the denoising capability of HRPCA, a laboratory experiment is first conducted on a five-story building model where the reference clean signal is aware. Then real-world monitoring data with varying degrees of outliers (e.g., single outlier, multiple outliers, and periodic outliers) collected from a cable-stayed bridge and a high-rise structure is used to further illustrate the efficiency of the proposed approach.

KEYWORDS

data cleaning, Hankel-structured robust principal component analysis (HRPCA), removal of gross outliers, structural health monitoring (SHM), structured low-rank representation

1 | INTRODUCTION

With the rapid growth of sensing technologies, a multitude of structural health monitoring (SHM) systems have been implemented on vital civil infrastructure to perform continuous condition monitoring.[1–4] As a result, huge amounts of valuable and precious monitoring data are collected, which allow for structural damage detection and in-service life prediction.[5,6] Before that, the accuracy of the data must be guaranteed. Unfortunately, due to the harsh measurement environment, noise inevitably exists in the sensed data. Its existence may greatly influence the results of structural health assessment and lead to false alarm.[7] As an example, Figure 1 shows 19-hour acceleration data of the Canton Tower recorded from 00:00 to 19:00 on July 26, 2020. The measured data was heavily contaminated by gross outliers, posing a barrier to subsequent data analysis and structural health evaluation. Therefore, soon after measurement, data cleaning must be performed by means of advanced signal denoising methods.[8]

The existing denoising methods in the SHM community could be broadly classified into four categories: filter-based methods,[9,10] wavelet-based methods,[11–13] singular value decomposition (SVD)-based methods,[14–17] or their combination.[18,19] The filter-based denoising methods, such as low-pass filter or band-pass filter, could reduce noise in a certain frequency range, but they may filter out some useful signal components due to the overlapping of signal and noise in the frequency domain. Compared with this category, the wavelet-based methods provide a better separation of noise and signal in the wavelet domain due to their strong ability in time-frequency analysis. For the third category, the SVD-based methods denoise a noisy signal by preserving large singular values while discarding small ones. Yet SVD is mainly devoted to removing small and dense Gaussian noise. These methods may face challenges in handling gross outliers, which often exist in real-world SHM data due to sensor malfunction, unreliable data transmission, and harsh electromagnetic environment.[20]

With the explosive advances in machine learning, researchers have recently pursued deep-learning-based techniques for outlier detection.[21–25] Bao et al.[21] combined computer vision and deep learning to detect gross outliers, where the raw time-series signals were first visualized and converted into image data and then these images were fed into a deep neural network (DNN) in the training stage for outlier detection. Tang et al.[22] proposed a convolutional neural network (CNN)-based method to improve the detection accuracy by training both time and frequency domain features of measurement data. Fu et al.[23] employed the similarity of power spectral density to detect sensor fault, and the monitoring data as input was fed into an artificial neural network (ANN) to identify different types of sensor fault, including gross outliers (spikes), drift, and bias. Arul and Kareem[24] detected outliers by using the shapelet transform and random forest classifier. However, most of the above neural networks are trained in a supervised manner, which means that labeled data is required in the training stage.

Another path for denoising signals with gross outliers is addressed in an unsupervised manner, such as subspace-based methods.[26] It is assumed that data can be projected or embedded into a low-dimensional subspace in which normal data would be better separated from gross outliers.[27] For example, Yang and Nagarajaiah[28] proposed a subspace-based method for denoising signals with gross outliers via the principal component pursuit (PCP) algorithm. By performing a matrix-reshape scheme, the clean data can be projected into a low-dimensional subspace represented as a low-rank matrix, while the gross outliers are represented as a sparse matrix. The denoised signal is then recovered from the low-rank matrix.

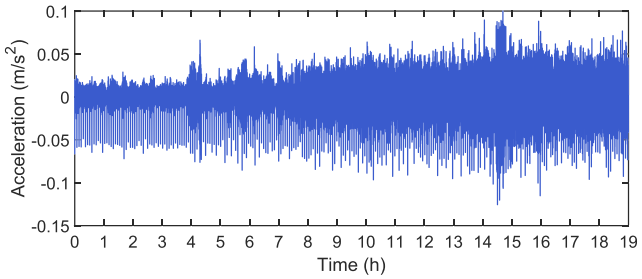

FIGURE 1 The recorded acceleration response on the Canton Tower from 00:00 to 19:00 on July 26, 2020, heavily contaminated by gross outliers

However, the subspace-based methods are highly reliant on the condition that there exists a low-dimensional subspace, which can represent the original clean response data. To satisfy this condition, an ingenious matrix construction scheme should be pursued. Recently, an annihilating filter-based low-rank Hankel matrix approach has been proposed by Jin et al.[29] They proved that there is a fundamental duality between the sparsity in transform domain and the low rankness in reciprocal domain. Specifically, if a signal is sparse in a transform domain, the associated Hankel matrix in the reciprocal domain is low rank. Premised on this duality, extensive applications on data recovery, data denoising, and compressed sensing have been successfully developed in the medical field for harnessing image signals.[30–36] To the best of the authors' knowledge, this duality has not been used in handling structural dynamic response data collected from SHM systems.

In the present study, a novel methodology termed Hankel-structured robust principal component analysis (HRPCA) will be developed for denoising structural dynamic response data contaminated with gross outliers. Making use of the fundamental duality, a low-dimensional (low-rank) subspace could be constructed to represent the originally redundant yet relevant structural dynamic response data, which allows for better separation of gross outliers embedded in the monitoring data. The primary contribution of this study is threefold: (i) structured low-rank approximation is introduced in the realm of SHM for removing gross outliers in monitoring data; (ii) in order to guarantee low rankness of the monitoring data, an annihilating filter-based fundamental duality is exploited to characterize the correlations among data; and (iii) the proposed HRPCA method enables not only outlier identification and removal but also recovery of fault data. In the remainder of this article, Section 2 introduces the proposed HRPCA method. Section 3 presents an experimental study on evaluating the performance of HRPCA. In Section 4, the robustness of the proposed method is further verified using real-world monitoring data collected from a cable-stayed bridge and a high-rise structure. Conclusions are drawn in Section 5.

2 | HANKEL-STRUCTURED ROBUST PRINCIPAL COMPONENT ANALYSIS (HRPCA)

2.1 | Matrix construction scheme of dynamic response data

Regarding structural dynamic response data collected by an SHM system, the relevant information often lies in a hidden low-dimensional subspace, leading to a great interest in representing the data with low-rank approximation. However, using only the rank-deficient property of SHM data is oftentimes insufficient. To fully utilize the spatial and temporal correlation in SHM data, additional structures of the data matrix need to be carefully exploited, such as Hankel and Toeplitz structure. Therefore, this section addresses the construction of a structured low-rank matrix that is nearest to represent the original redundant yet relevant data, where both the Hankel and rank-deficiency properties of the data are explored.

The structural dynamic response data measured from a sensor can be represented as a one-dimensional time-domain signal $x(t)$. Since only limited structural natural frequencies can be excited by external inputs, $x(t)$ has a sparse spectrum in the frequency domain. Thus, the corresponding one-dimensional frequency-domain counterpart $\widehat{x}(\omega)$ can be expressed as

$$\widehat{x}(\omega) = \mathcal{F}\{x(t)\} = \sum_{j=1}^{k} c_j \delta(\omega - \omega_j) \tag{1}$$

where $\mathcal{F}\{\cdot\}$ denotes the Fourier transform; k denotes the number of excited frequencies in the structural response, which is also the number of nonzero components of $\widehat{x}(\omega)$; ω_j and c_j denote the location and amplitude of nonzero components; $\delta(\cdot)$ denotes the Dirac function. According to Equation 1, the frequency-domain signal $\widehat{x}(\omega)$ can be said to be k-sparse.

As $\widehat{x}(\omega)$ has sparse nonzero values at locations $\{\omega_j\}_{j=1}^{k}$, it is easy to define an annihilating function $\widehat{h}(\omega)$ in the frequency domain, with $\widehat{h}(\omega)$ being equal to zero at the locations $\{\omega_j\}_{j=1}^{k}$, such that the signal $\widehat{x}(\omega)$ is annihilated by the annihilating function $\widehat{h}(\omega)$[37,38]:

$$\widehat{h}(\omega)\widehat{x}(\omega) = 0, \forall \omega \tag{2}$$

By taking inverse Fourier transform on Equation 2, we have the following expression:

$$h(t) * x(t) = 0, \forall t \tag{3}$$

where $*$ denotes the convolution operator; $h(t)$ is referred to as the annihilating filter in time domain.[38] For example, if $x(t) = sin(\omega_0 t)$ is a sinusoidal signal with frequency ω_0, then, it can be annihilated by a filter with a notch at ω_0. A pictorial illustration of annihilating filter is given in Figure 2.

The continuous signal $x(t)$ and the annihilating filter $h(t)$ can be discretized at Nyquist sampling rates. The corresponding discrete forms can be expressed as $x[n] = x(n\Delta t)$ and $h[n] = h(n\Delta t)$, respectively, in which Δt is the sampling interval. Then, the discrete form of Equation 3 can be written as

$$h[n] * x[n] = \sum_{l=-\infty}^{+\infty} h[l]x[n-l] = 0, n \in \mathbb{Z} \tag{4}$$

Indeed, there are many choices of annihilating function $\widehat{h}(\omega)$ that satisfies Equation 2. Among them, Vetterli et al.[38,39] demonstrated that an annihilating function can be constructed using a finite combination of sinusoidal functions, such that the corresponding discrete annihilating filter has a finite filter length. Thus, if a signal is k-sparse in the frequency domain, we can choose an annihilating filter that has a finite length m with the minimum length of $k+1$ (i.e., $m \geq k+1$). Then, Equation 4 can be converted into matrix form as

$$\mathcal{L}(x)\overline{VEC(h)} = \mathbf{0} \tag{5}$$

in which,

$$\mathcal{L}(\mathrm{x}) = \begin{bmatrix} \vdots & \vdots & \ddots & \vdots \\ \mathrm{x[0]} & \mathrm{x[1]} & \cdots & \mathrm{x[m-1]} \\ \mathrm{x[1]} & \mathrm{x[2]} & \cdots & \mathrm{x[m]} \\ \mathrm{x[2]} & \mathrm{x[3]} & \cdots & \mathrm{x[m+1]} \\ \vdots & \vdots & \ddots & \vdots \\ \mathrm{x[n-m+1]} & \mathrm{x[n-m+2]} & \cdots & \mathrm{x[n]} \\ \mathrm{x[n-m+2]} & \mathrm{x[n-m+3]} & \cdots & \mathrm{x[n+1]} \\ \vdots & \vdots & \ddots & \vdots \end{bmatrix}, \overline{\mathrm{VEC(h)}} = \begin{bmatrix} \mathrm{h[m]} \\ \vdots \\ \mathrm{h[2]} \\ \mathrm{h[1]} \end{bmatrix}$$

where m is the length of the filter $h[n]$, which is longer than the sparsity level of $\widehat{x}(\omega)$, that is, $m \geq k+1$; $\overline{VEC(h)}$ is the reverse order of the filter $h[n]$.If we only consider the valid convolution herein by removing the boundary data outside of $x[1], \cdots, x[n]$, the following matrix equation can be obtained:

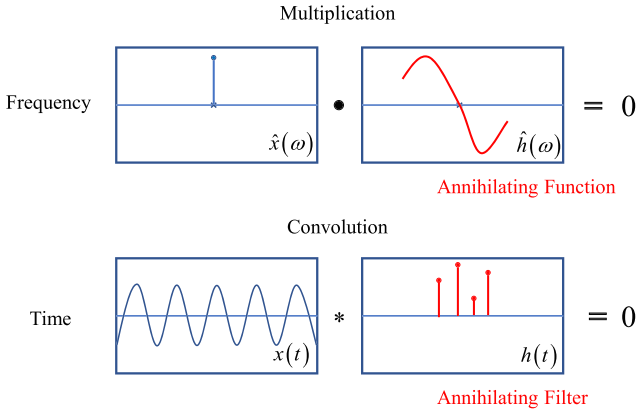

FIGURE 2 A pictorial example of annihilating filter

$$\mathcal{H}(x)\overline{VEC(h)} = \mathbf{0} \tag{6}$$

where the notation $\mathcal{H}(x)$ denotes the Hankel-structured operator (each ascending skew diagonal from left to right remains constant), which is constructed as

$$\mathcal{H}(x) = \begin{bmatrix} x[1] & x[2] & \cdots & x[m] \\ x[2] & x[3] & \cdots & x[m+1] \\ \vdots & \vdots & \ddots & \vdots \\ x[n-m+1] & x[n-m+2] & \cdots & x[n] \end{bmatrix} \tag{7}$$

here, n will be chosen to ensure $n-m+1>k$.

Equation 6 implies that the constructed Hankel matrix $\mathcal{H}(x)$ is low rank. Furthermore, Jin et al.[29] mathematically proved that the rank of $\mathcal{H}(x)$ will always equal to the sparsity level of $\widehat{x}(\omega)$ if the conditions $m \geq k+1$ and $n-m+1>k$ are satisfied. This suggests the following fundamental duality:[29–35]

$$k\text{-sparse signal in frequency domain} \overset{\mathcal{F}}{\Longleftrightarrow} k\text{-ranked Hankel structured matrix}$$

Based on the above duality, it is found that if $x(t)$ is a time series obtained from a structure with sparse frequency property, then the enlarged Hankel matrix of $x(t)$ is low rank. It will be applied in the next section to conduct signal denoising for structural dynamic response data with gross outliers.

2.2 | Denoising monitoring data with gross outliers

The measured structural response data with gross outliers can be expressed as

$$\mathbf{Y} = \mathbf{X} + \mathbf{E} \tag{8}$$

where $\mathbf{Y} = \{y[1], y[2], ..., y[n]\}$ denotes the measured data; $\mathbf{X} = \{x[1], x[2], ..., x[n]\}$ denotes the 'clean' structural dynamic response data; $\mathbf{E} = \{e[1], e[2], ..., e[n]\}$ denotes the gross outliers; n is the number of sample points. Because gross outliers arise from the sensor imperfection or environmental interference, only a small subset of data would be affected. Therefore, $\mathbf{E}$ is sparse but with gross and arbitrarily large magnitudes.

For the outlier-corrupted measurement vector $\mathbf{Y} = \{y[1], y[2], ..., y[n]\}$, we build the Hankel matrix $\mathcal{H}(\mathbf{Y})$ of size $(n-m+1)\times m$ as

$$\mathcal{H}(\mathbf{Y})_{(n-m+1)\times m} = \begin{bmatrix} y[1] & y[2] & \cdots & y[m] \\ y[2] & y[3] & \cdots & y[m+1] \\ \vdots & \vdots & \ddots & \vdots \\ y[n-m+1] & y[n-m+2] & \cdots & y[n] \end{bmatrix} \tag{9}$$

in which $n-m+1>k$ and $m \geq k+1$. In the noiseless scenario, the matrix $\mathcal{H}(\mathbf{Y})$ would be a Hankel matrix of rank k. However, such low-rank Hankel structure will be broken in the presence of outliers in the measurement.

On this basis, the constructed observation matrix $\mathcal{H}(\mathbf{Y})$ can be regarded as superposition of a low-rank matrix $\mathcal{H}(\mathbf{X})$ and a sparse matrix $\mathcal{H}(\mathbf{E})$:

$$\mathcal{H}(\mathbf{Y}) = \underbrace{\mathcal{H}(\mathbf{X})}_{low\ \text{rank}} + \underbrace{\mathcal{H}(\mathbf{E})}_{sparse} \tag{10}$$

in which $\mathcal{H}(\mathbf{X})$ represents the Hankel form of $\mathbf{X}$. Since the clean response data $\mathbf{X}$ is sparse in frequency domain, the constructed Hankel matrix $\mathcal{H}(\mathbf{X})$ is low rank according to the duality described in Section 2.1. Meanwhile, $\mathcal{H}(\mathbf{E})$ remains sparse because organizing a sparse vector$\mathbf{E}$ into a Hankel matrix would not essentially change its sparse property. Hence, the outliers could cluster in sparse component $\mathcal{H}(\mathbf{E})$ rather than scatter across the whole data matrix.

So far, the problem of denoising gross outliers is mathematically formulated as a decomposition of $\mathcal{H}(\mathbf{Y})$ into a low-rank matrix $\mathcal{H}(\mathbf{X})$ and a sparse matrix $\mathcal{H}(\mathbf{E})$. In fact, decomposing a matrix into two unknown components is difficult if there are no other constraints. However, the matrices $\mathcal{H}(\mathbf{X})$ and $\mathcal{H}(\mathbf{E})$ are subjected to the constraint of low rankness and sparsity, as shown in Equation 10. As such, Equation 10 can be addressed by RPCA, which leads to the following optimization problem[40,41]:

$$\begin{aligned} (\mathrm{P1}): \quad & \min rank\{\mathcal{H}(\mathbf{X})\} + \lambda \|\mathcal{H}(\mathbf{E})\|_0 \\ & \text{subject to } \mathcal{H}(\mathbf{Y}) = \mathcal{H}(\mathbf{X}) + \mathcal{H}(\mathbf{E}) \end{aligned} \tag{11}$$

in which, $rank\{\cdot\}$ is the operator calculating the rank of a matrix; $\|\cdot\|_0$ is the ℓ_0-norm, which denotes the number of nonzero elements in a matrix; λ is a parameter of trade-off between the low-rank and sparse components. Compared with classical PCA, the merit of RPCA is its strong ability in handling gross and sparse outliers. Hence, in this study, it is more appropriate to solve Equation 11 using RPCA instead of PCA.[40]

The problem (P1) could be interpreted as finding the optimal approximations of $\mathcal{H}(\mathbf{X})$ with the smallest rank and $\mathcal{H}(\mathbf{E})$ with the sparsest representation from the corrupted data matrix $\mathcal{H}(\mathbf{Y})$. However, the optimization problem (P1) is nonconvex, which is tricky to solve. To develop a tractable formulation, Equation 11 can be solved by optimizing the following convex problem:

$$\begin{aligned} (\mathrm{P}*): \quad & \min \|\mathcal{H}(\mathbf{X})\|_* + \lambda \|\mathcal{H}(\mathbf{E})\|_1 \\ & \text{subject to } \mathcal{H}(\mathbf{Y}) = \mathcal{H}(\mathbf{X}) + \mathcal{H}(\mathbf{E}) \end{aligned} \tag{12}$$

where $\|\cdot\|_*$ denotes the nuclear norm, representing the summation of the singular values of a matrix; $\|\cdot\|_1$ denotes the ℓ_1-norm. The problem (P*) can be optimized by using the alternating direction method of multipliers (ADMM), because of its high guarantee for getting a global minimization.

Once the optimal approximations $\mathcal{H}(\mathbf{X})^*$ and $\mathcal{H}(\mathbf{E})^*$ are obtained from Equation 12, the denoised structural response data $\mathbf{X}^*$ with the size of $1 \times n$ can be reshaped back, which is expressed as

$$\mathbf{X}^* = \mathcal{H}^{-1}(\mathcal{H}(\mathbf{X})^*) \tag{13}$$

in which, $\mathcal{H}^{-1}$ is the inverse Hankel operator.

For pictorial description of the proposed HRPCA denoising method, the implementation procedures are summarized below and in Figure 3.

Step 1:	Choose an appropriate filter length m.
Step 2:	Organize the outlier-corrupted measurement data $\mathbf{Y}_{1\times n}$ into Hankel matrix $\mathcal{H}(\mathbf{Y})_{(n-m+1)\times m}$ according to Equation 9.
Step 3:	Decompose Hankel matrix $\mathcal{H}(\mathbf{Y})$ into a superposition of a low rank $\mathcal{H}(\mathbf{X})$ and a sparse component $\mathcal{H}(\mathbf{E})$ by using the RPCA according to Equation 12.
Step 4:	Obtain the denoised structural response data $\mathbf{X}^*_{1\times n}$ via inverse Hankel operator according to Equation 13.

In implementing the above procedures, two parameters, that is, the length of the annihilating filter m and the trade-off parameter λ, need to be appropriately selected. The selection criteria of the two parameters will be elaborated according to the parameter analysis given in Section 3.4.

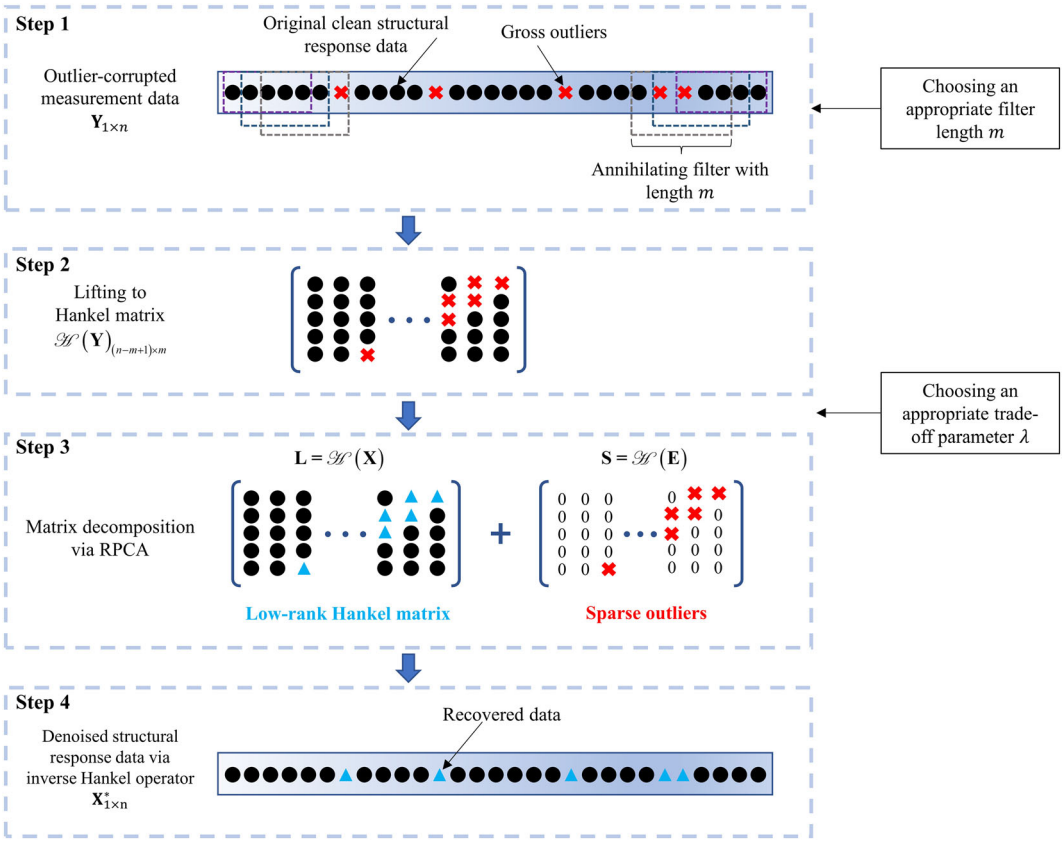

FIGURE 3 Visualization illustration of the proposed HRPCA approach

3 | EXPERIMENTAL VALIDATION

3.1 | Experiment setup

The measured dynamic response data obtained from vibration tests of a five-story building model as shown in Figure 4 are first used to experimentally verify the efficacy of the proposed denoising approach. The building model consists of five steel floors with size of 600 × 400 × 15 mm and four equal rectangular columns with cross section of 50 × 6 mm.[42] The total height of the model is 1000 mm with identical height for each story. Silicon oil dampers are installed on the structure to increase the damping of the model. To measure the excitation and structural dynamic responses, a total of four displacement meters, nine accelerometers, and one force sensor are installed on the tested structure, with the sampling frequency of 600 Hz. The sensor layout is shown in Figure 4b.

During the experiment, two types of excitations are imposed on the tested structural model. One is periodic excitations acting on the first and fifth floors, leading to stationary structural dynamic responses. The other is hammer excitation acting at the top floor, leading to nonstationary structural dynamic responses.

The acceleration response acquired on the top floor is referred as original clean signal (benchmark signal), and subsequently, it is artificially corrupted by gross outliers to generate outlier-corrupted response data. Hence, the performance of the proposed denoising method could be verified by comparing the denoised acceleration data with the original clean data. In this study, a typical impulsive noise model, called the Middleton Class-A Noise, is adopted to simulate the gross outliers in the response data, which could be described by its probability density function (PDF) as[43,44]

$$f_Z(z)=\sum_{i=0}^{\infty}\frac{p_i}{\sqrt{2\pi\sigma_i^2}}exp\left(-\frac{z^2}{2\sigma_i^2}\right) \tag{14}$$

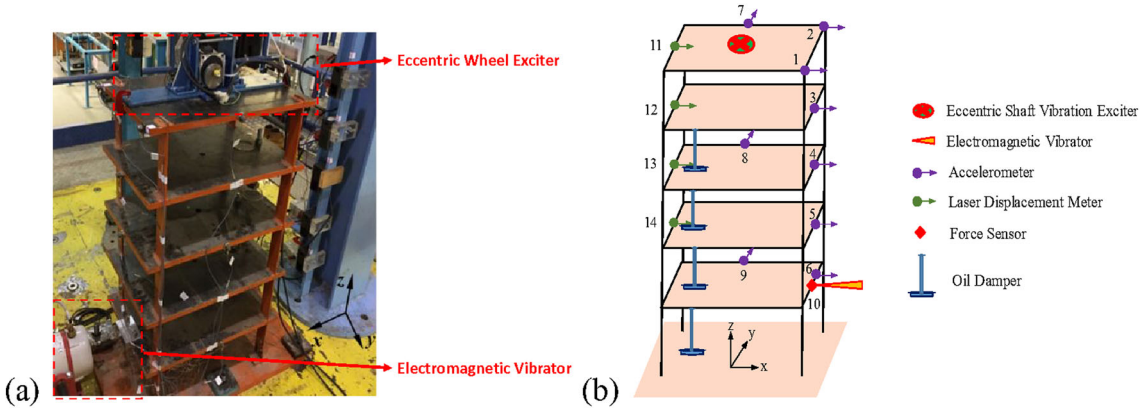

FIGURE 4 (a) Experimental setup of the tested structural model; (b) layout of sensors and vibration exciters

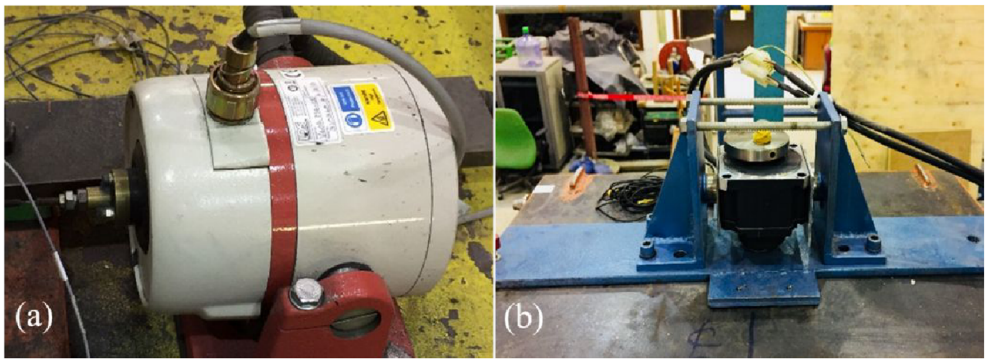

FIGURE 5 (a) Electromagnetic vibrator; (b) eccentric wheel exciter

in which $p_i = \left(e^{-A}A^i\right)/i!$ is the steady-state probability of the ith impulsive source and $\sigma_i^2 = \left(\frac{i}{A}+\Gamma\right)/(1+\Gamma)$ is the variance of impulsive source. The Class-A Noise model is characterized by the parameters A and Γ: the impulsive index A represents the amount of impulsiveness, and the scale factor Γ denotes a ratio of the power of the Gaussian component to that of the non-Gaussian components. A large value of A means that the noise could be generated arbitrarily close to Gaussian, while a small value of A implies that the noise could be generated close to a conventional Poisson process. In this study, the parameters of the Middleton Class-A Noise model are set as $A = 0.005$ and $\Gamma = 10^{-6}$, making the generated noise highly impulsive.

3.2 | Analysis of results

3.2.1 | Stationary response under periodic excitation

Under two periodic excitations with frequencies of 2 Hz (generated by an electromagnetic vibrator installed on the first floor, Figure 5a) and 10 Hz (generated by an eccentric wheel exciter installed on the fifth floor, Figure 5b), the time series of acceleration response at the fifth floor and the corresponding spectrum in frequency domain are shown in Figures 6a and 6b. Here, the measured acceleration response is regarded as original clean signal and denoted as $\mathbf{X}$. It is apparent that $\mathbf{X}$ is sparse in the frequency domain. Hence, according to the duality described in Section 2.1, the proposed matrix construction scheme can be implemented on $\mathbf{X}$ such that the constructed Hankel matrix $\mathcal{H}(\mathbf{X})$ is low rank. Figures 6c and 6d show the additive gross outliers $\mathbf{E}$ artificially generated by the Middleton Class-A Noise model in time and frequency domains, respectively. It is seen that $\mathbf{E}$ has a flat spectral distribution in frequency domain, making it difficult to separate or filter out $\mathbf{E}$ by applying frequency-based or time-frequency-based methods. After adding $\mathbf{E}$ into $\mathbf{X}$, Figures 6e and 6f illustrate the synthetic outlier-corrupted signal $\mathbf{Y}$ in time and frequency domains. The target is

to remove the gross outliers $\mathbf{E}$ from the outlier-corrupted signal $\mathbf{Y}$ and elicit the clean signal $\mathbf{X}$ by use of the proposed HRPCA method.

When organizing the outlier-corrupted data $\mathbf{Y}$ into Hankel matrix, the size of the Hankel matrix $\mathcal{H}(\mathbf{Y})$ needs to be larger than the sparsity level of $\mathbf{X}$, such that $m \geq k+1$ and $n-m+1>k$. To satisfy this condition, the length of the annihilating filter is set as $m=100$, because the sparsity level $(k=2)$ observed from Figure 6b is much smaller than 100. In reality, relatively few vibration modes are excited in structural dynamic responses, resulting$k \ll 100$. Therefore, the length of the annihilating filter is fixed at $m=100$ for all experimental studies presented in this paper. The trade-off parameter λ is set as 0.032 (a discussion on the influence of λ on the denoising performance and the determination of its optimal value will be detailed in Section 3.4 later).

Figure 7 shows the denoising results by HRPCA under periodic excitations. The blue line is the original clean signal $\mathbf{X}$, the black line is the outlier-corrupted signal $\mathbf{Y}$, and the red dot line denotes the denoised signal $\mathbf{X}^*$ by HRPCA. It can be seen that gross outliers in the corrupted signal have been satisfactorily removed with high efficiency. The denoised signal (red dot line) matches pretty well with the original clean signal (blue line) and the error (green line) between them is almost zero, implying that $\mathbf{X}$ has been perfectly recovered from $\mathbf{Y}$ without losing much information. The power spectral densities (PSDs) of the original clean signal and denoised signal are also presented in Figure 7. By comparing them with the PSD of the outlier-corrupted signal shown in Figure 6f, it is seen that the outliers $\mathbf{E}$ distributed along the whole frequency band have been well removed, demonstrating the capability of the proposed HRPCA method in handling outliers with its appearance as broadband noises.

3.2.2 | Nonstationary response under hammer excitation

In most of real excitation scenarios such as wind loadings or earthquakes, the structural dynamic responses often exhibit nonstationary behaviors, which may affect the performance of denoising methods.[45] So, we next examine the performance of the proposed denoising method in handling nonstationary response data. To obtain such data, the tested structural model is subjected to hammer excitation at the fifth floor, and nonstationary structural dynamic response data are collected. Similarly, the measured acceleration response at the top floor is referred as the clean response data, which is denoted as $\mathbf{X}$. The gross outlier data $\mathbf{E}$ created by the Middleton Class-A Noise model is added in $\mathbf{X}$ to generate outlier-corrupted acceleration response data $\mathbf{Y}$. The data sets of $\mathbf{X}$, $\mathbf{E}$, and $\mathbf{Y}$ in both time and frequency domains are illustrated in Figure 8.

Similarly, as shown in Figure 8(b), the sparseness of $\mathbf{X}$ in frequency domain implies that the Hankel structure of the original response in time domain $\mathcal{H}(\mathbf{X})$ is low rank. Thus, the proposed denoising method can still be implemented to recover the nonstationary response data $\mathbf{X}$ from the outlier-corrupted measurements $\mathbf{Y}$. In this scenario, the trade-off parameter $\lambda=0.1$ and the annihilating filter length $m=100$ are selected, and the denoising results are shown in Figure 9. The results clearly indicate that the proposed method removes the gross outliers $\mathbf{E}$ from the corrupted measurements $\mathbf{Y}$ effectively, implying that HRPCA is also efficient to denoise the nonstationary response data with gross outliers.

3.3 | Comparison of denoising performance with existing methods

In this section, the denoising performance of HRPCA is compared with four existing signal denoising methods: median filter, wavelet, SVD, and PCP. The median filter is implemented by a built-in algorithm in MATLAB®, named as 'medfilt1'. The wavelet method is implemented by canceling all wavelet coefficients that exceed the universal threshold.[46] For comprehensive verification, a wavelet of the Symlet family (order 6) under different decomposition levels are considered (J = 1,2 ...,5). For the SVD-based method, the first k-singular values are extracted by minimizing the squared error between the original signal and the denoised one.[47] In PCP, we use the default parameter setting suggested by Yang and Nagarajaiah.[28] The main difference between PCP and HRPCA lies in the different matrix construction schemes of dynamic response data. In practice, an SHM data matrix can be very 'thin' with many time steps (rows) and relatively few channels (columns), which is sometimes full rank or not so low rank. To formulate a low-rank representation of SHM data, a matrix-reshape scheme is adopted in PCP to ensure the low-rank representation of SHM data.[28] Specifically, the original 'thin' matrix is reshaped into a 'square' matrix to ensure redundancy. In contrast, HRPCA adopts Hankel matrix construction scheme to ensure the low-rank representation of SHM data. By organizing the SHM

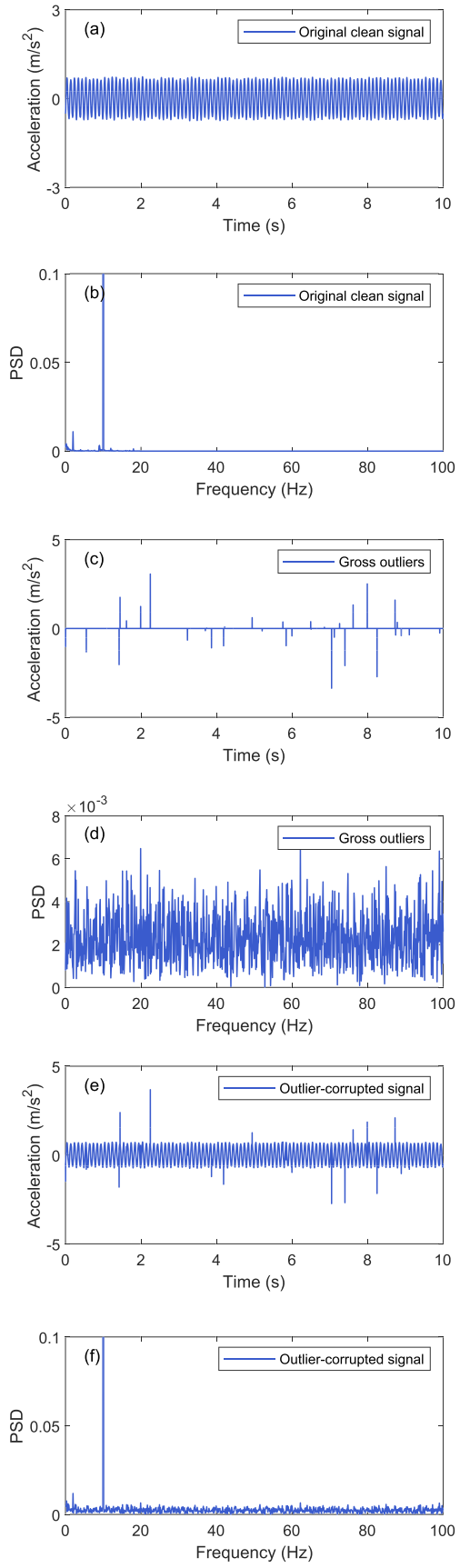

FIGURE 6 (a–b) Original clean signal **X** in time and frequency domains; (c–d) additive gross outliers**E** in time and frequency domains; (e–f) synthetic outlier-corrupted signal **Y** in time and frequency domains

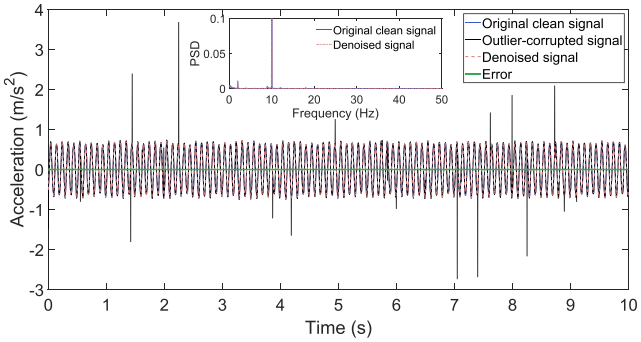

FIGURE 7 Denoising performance of the proposed method for stationary response

data into Hankel matrix, the constructed Hankel matrix would be low rank. Compared to PCP, HRPCA exploits the fundamental duality to construct the low-rank Hankel matrix, which has stronger theoretical and mathematical support.

Two evaluation metrics, namely, the signal to noise ratio (SNR) and the percentage root mean square difference (PrmsD), are chosen to quantitatively compare the above methods. SNR and PrmsD are defined as

$$SNR = 10 \times log_{10} \frac{\sum_{i=1}^{n} x[i]^2}{\sum_{i=1}^{n} (x[i] - x^*[i])^2} \tag{15}$$

$$\text{PrmsD} = 100 \times \sqrt{\frac{\sum_{i=1}^{n} (x[i] - x^*[i])^2}{\sum_{i=1}^{n} x[i]^2}} \tag{16}$$

in which $\mathbf{X} = \{x[1], x[2], ..., x[n]\}$ denotes the clean response data and $\mathbf{X}^* = \{x^*[1], x^*[2], ..., x^*[n]\}$ denotes the denoised response data obtained by one of the above methods; n is the total number of data points. Larger values of SNR and smaller values of PrmsD indicate a better denoising performance.

To obtain a clear picture of the denoising performance, the values of SNR and PrmsD obtained by different methods are summarized in Table 1. It can be found that (i) the proposed HRPCA method, which yields the largest SNR and smallest PrmsD, exhibits the best denoising performance among five denoising methods, both for stationary and nonstationary responses; (ii) the denoising performance of all five methods for stationary response is better than that for nonstationary response; (iii) PCP has excellent denoising performance (only slightly worse than HRPCA) in stationary response scenario and outperforms the median filter, SVD, and wavelet; however, it works worst among five methods in denoising the nonstationary response. This is possibly because of the adoption of a matrix-reshape scheme to ensure the low-rank representation of SHM data in this method.[28] For stationary responses, such a matrix-reshape scheme could be effective to form a low-rank matrix. However, for nonstationary responses, simply changing the shape of a matrix may not significantly improve the low-rank characteristic of this matrix; (iv) unlike PCP, the median filter has relatively good denoising performance in both stationary and nonstationary response scenarios, which can also be satisfactory in some practical applications. The denoising performance of SVD is too poor to work in both scenarios; and (v) among the five different decomposition levels of wavelet, decomposing the stationary response into three levels and decomposing the nonstationary response into one level perform the best, but only slight improvement is made when compared to the corrupted signal. Moreover, in real applications, it is work intensive to determine the level of wavelet decomposition with a view to achieve favorable denoising performance. In summary, the proposed HRPCA method could remove gross outliers effectively in both stationary and nonstationary response scenarios while preserving the original clean signal with high accuracy and fidelity.

3.4 | Parameter analysis

In the proposed denoising method, two key parameters, that is, the length of the annihilating filter m and the trade-off parameter λ, need to be determined. In this section, the influence of these two parameters on the proposed denoising method is discussed, and some suggestions on the selection of the parameters in practical applications are provided.

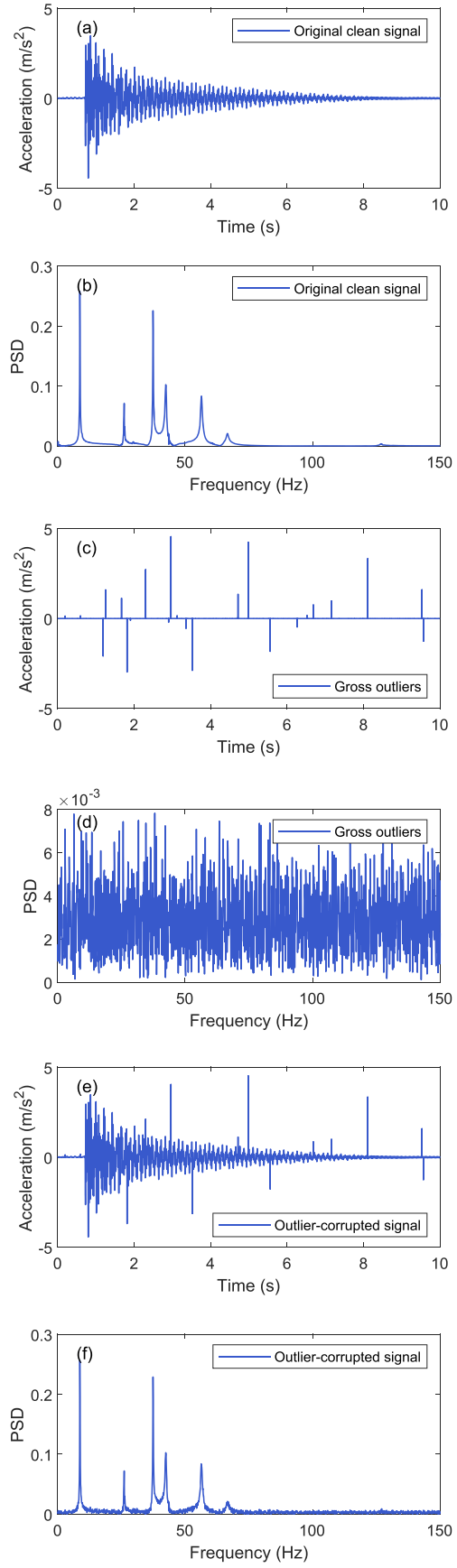

FIGURE 8 (a–b) Original clean signal **X** in time and frequency domains; (c–d) additive gross outliers**E** in time and frequency domains; (e–f) synthetic outlier-corrupted signal **Y** in time and frequency domains

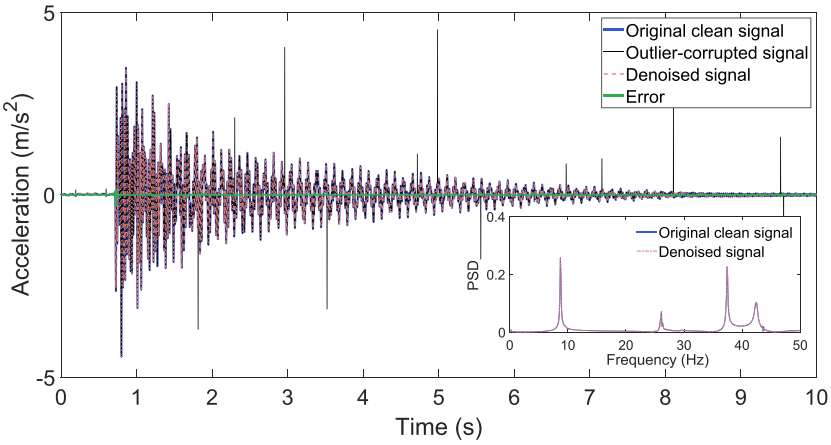

FIGURE 9 Denoising performance of the proposed method for nonstationary response

TABLE 1 Summary of denoising performance for different methods

Denoising methods		Stationary response		Nonstationary response	
		SNR (dB)	PrmsD (%)	SNR (dB)	PrmsD (%)
Corrupted signal		13.55 dB	21.00%	11.62 dB	26.24%
Median filter		39.46 dB	1.06%	29.23 dB	3.46%
Wavelet	J = 1	15.92 dB	15.99%	14.57 dB	18.68%
	J = 2	19.19 dB	10.98%	14.24 dB	19.41%
	J = 3	21.36 dB	8.55%	4.87 dB	57.08%
	J = 4	19.04 dB	11.17%	3.35 dB	68.00%
	J = 5	1.79 dB	81.29%	2.44 dB	75.52%
SVD		21.63 dB	8.29%	13.65 dB	20.76%
PCP		47.31 dB	0.43%	7.76 dB	40.91%
Proposed HRPCA		55.30 dB	0.17%	36.13 dB	1.56%

Figure 10 shows the performance of the proposed denoising method under different values of the filter length m and trade-off parameter λ, where the stationary response data given in Section 3.2.1 is selected for the analysis and the denoising performance is evaluated in terms of SNR. First, the influence of λ on the performance is discussed by analyzing the relationship between λ and SNR for a certain m. As can be seen from the obtained curves, the trade-off parameter λ shows a great influence on the SNR value, which means that the accuracy of the proposed denoising method depends on an appropriate selection of λ. Candès et al.[40] proposed a universal selection criterion for λ, that is, $\lambda = 1/\sqrt{\max(n_1, n_2)}$, where $n_1$andn_2 are the dimensionality of the constructed data matrix $M \in \mathbb{R}^{n_1 \times n_2}$. However, λ is a data-dependent parameter[41] and therefore should be relevant to the sparsity level of the data matrix. As such, the λ value obtained by the universal selection criterion might not be the optimal one in reality. As shown in Figure 10, the λ values estimated by the two ways are a little bit different. The λ values (marked with circle) determined by the sparsity level of the data matrix achieve slightly higher SNR than those (marked with triangle) estimated by the universal selection criterion. Afterward, the influence of m on the performance is addressed by analyzing the relationship between SNR and m under the optimal λ. It turns out that the value of SNR does not change much even when m increases from 50 to 1000; in particular, the optimal value of λ is less affected by m, indicating that the proposed denoising method is insensitive to m.

Based on the above analysis, it is suggested that λ be determined by slightly tuning the value calculated from the universal selection criterion ($\lambda = 1/\sqrt{\max(n_1,n_2)}$), while m be chosen as long as the conditions $m \geq k+1$ and $n-m+1 > k$ are satisfied.

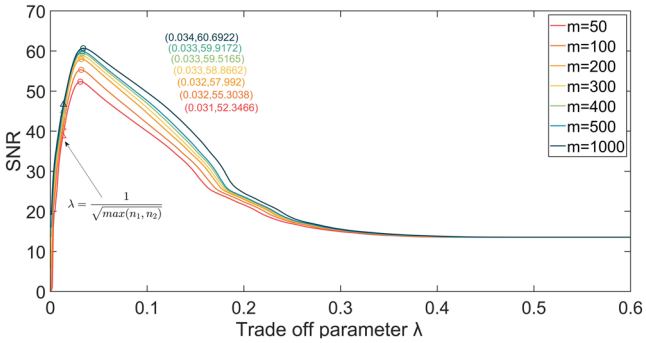

FIGURE 10 SNR versus trade-off parameter λ under different filter length m

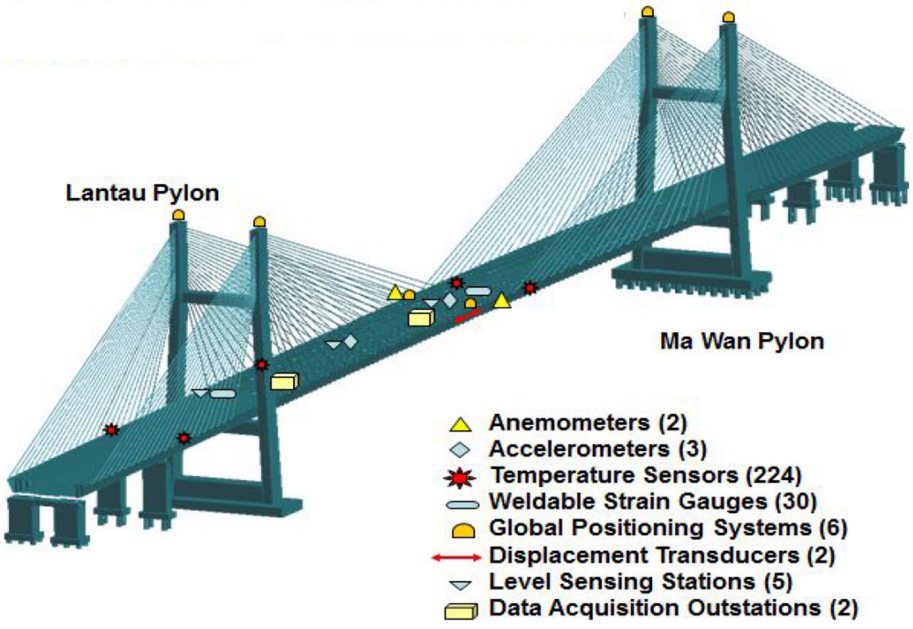

FIGURE 11 Sensor configuration of the SHM system deployed on KSMB[48]

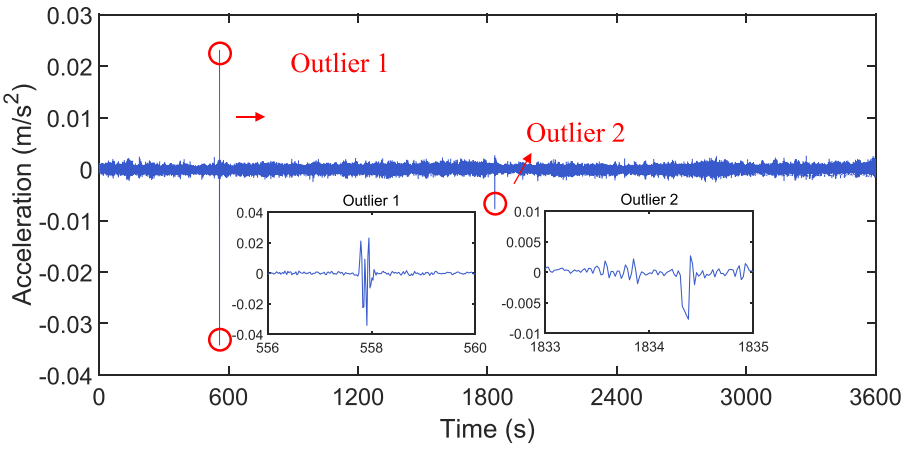

FIGURE 12 Measured acceleration response of KSMB (Case 1)

4 | APPLICATIONS TO REAL-WORLD SHM DATA

The experimental results have shown a good performance of the proposed HRPCA method for suppressing gross outliers and reconstructing clean signals. To verify its ability in real-world applications, four sets of SHM data with different outlier corruption degrees are considered in this section: two sets of in situ acceleration data (denoted as Case 1 and Case 2) collected from the Kap Shui Mun Bridge, two other sets of in situ acceleration data (denoted as Case 3 and Case 4) collected from the Canton Tower.

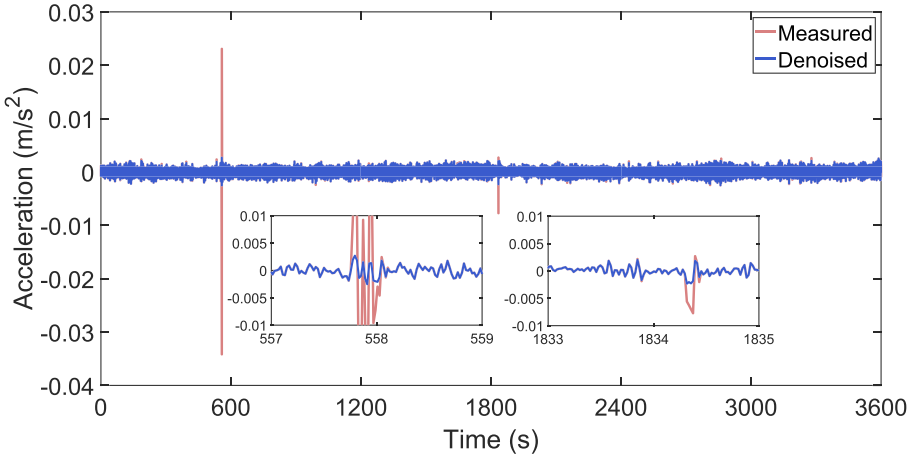

FIGURE 13 Denoised acceleration response of KSMB (Case 1)

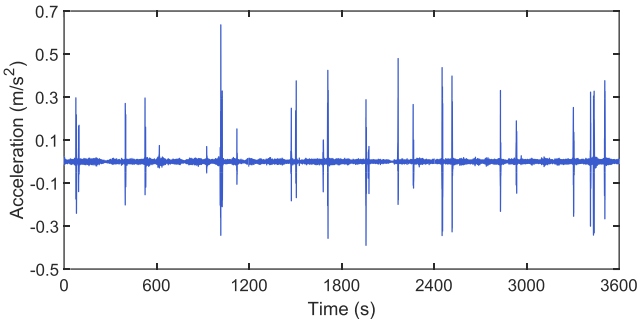

FIGURE 14 Measured acceleration response of KSMB (Case 2)

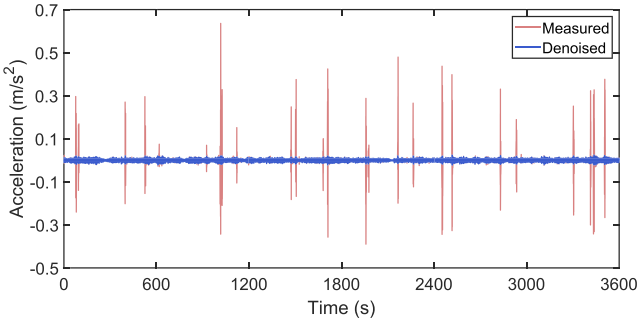

FIGURE 15 Denoised acceleration response of KSMB (Case 2)

4.1 | Application to Kap Shui Mun Bridge (KSMB)

The Kap Shui Mun Bridge, located between the islands of Lantau and Ma Wan in Hong Kong, is a cable-stayed bridge with a main span of 430 m and two side spans of 160 m on either side, carrying both road and railway traffic. To ensure its safety and integrity, a long-term SHM system, consisting of more than 270 sensors of various types, has been permanently installed on the bridge (Figure 11).[2,48] An immense amount of monitoring data has been collected by this system. Due to harsh operational and environmental conditions on the site, the measured data inevitably contains serious outliers, which adversely affect the usability of the data.

As an example, Figure 12 shows the acceleration data of KSMB collected at 7:00 to 8:00 on January 12, 2012 with the sampling frequency of 51.2 Hz (denoted as Case 1). As denoted by red circles, two abnormal data points referred as gross outliers are observed in the measured acceleration response data. The Outlier 2 shown in Figure 12 is easy to handle because it is a single spike, while the Outlier 1 shows multiple spikes with different amplitudes.

According to the discussion given in Section 3.4, we set the length of the annihilating filter $m = 100$ and the trade-off parameter $\lambda = 0.01$ in this case. The denoising results by the proposed method are shown in Figure 13. It is seen that the two gross outliers have been removed effectively, no matter whether the outliers have single or multiple spikes embedded in the signal. Moreover, the other normal data points are well retained without observable data loss, demonstrating the effectiveness of HRPCA in outlier removal and fault data recovery.

The second set of data (denoted as Case 2) is the acceleration response data collected at 14:00 to 15:00 on January 27, 2012, which is heavily contaminated by outliers. As shown in Figure 14, there are more than two dozen irregular outliers in 1-hour acceleration response time series, some of which are significantly larger than the normal responses. In such a case, effective denoising is necessary before pursuing structural health assessment by use of the monitoring

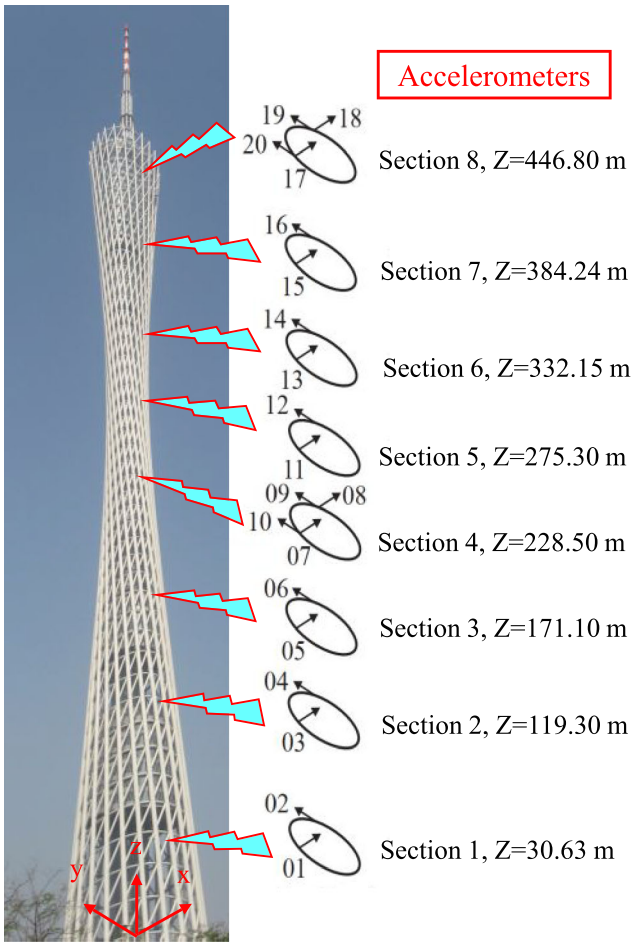

FIGURE 16 Deployment of accelerometers on Canton Tower

data. By applying the proposed HRPCA method ($m = 100$, $\lambda = 0.005$ in this case), all the outliers are successfully removed as shown in Figure 15, indicating that the proposed HRPCA method is also effective for handling multipoint irregular outliers.

4.2 | Application to Canton Tower

The field monitoring data collected from the Canton Tower is further used to verify the denoising performance of the proposed HRPCA method. The Canton Tower, located in the city of Guangzhou, China, is a supertall structure with a total height of 600 m. A sophisticated long-term SHM system consisting of more than 700 sensors has been installed on this supertall structure by the Hong Kong Polytechnic University.[3,49,50] As part of the deployed SHM system, a total of 20 uniaxial accelerometers were installed on eight levels of the tower at heights of 30.6, 119.3, 171.1, 228.5, 275.3, 332.2, 384.2, and 446.8 m, as shown in Figure 16. Four uniaxial accelerometers were installed on the 4th and 8th levels, while

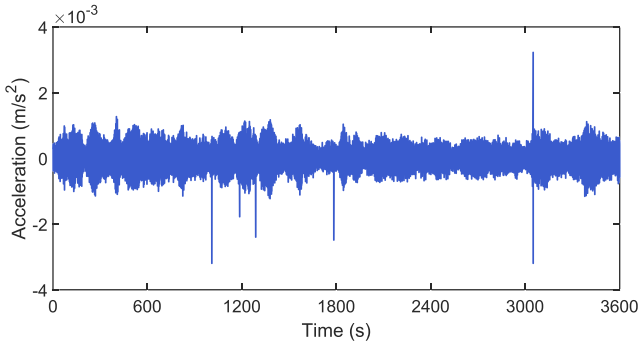

FIGURE 17 Measured acceleration response of Canton Tower (Case 3)

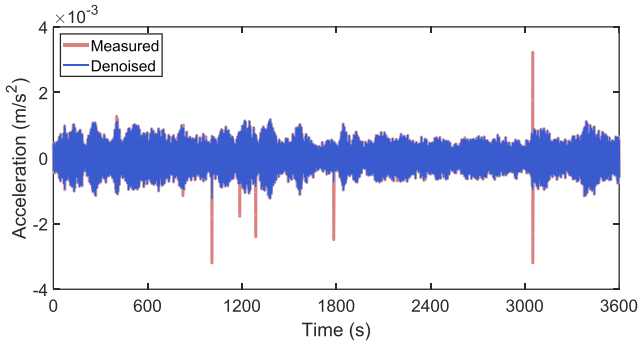

FIGURE 18 Denoised acceleration response of Canton Tower (Case 3)

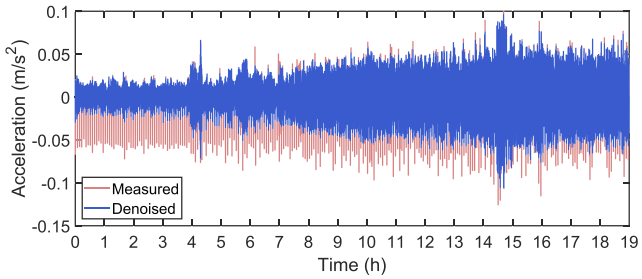

FIGURE 19 Denoised acceleration response of Canton Tower (Case 4)

on the other six levels, each cross section was equipped with two uniaxial accelerometers. The acceleration data was acquired by a data acquisition system at the sampling rate of 50 Hz.

Figure 17 shows a set of 1-h acceleration response of the Canton Tower collected at 11:00 to 12:00 on January 20, 2010, denoted as Case 3. It is observed that the signal has several gross outliers embedded. The amplitude and arrival time of every outlier are random, imposing biases for further analysis. Figure 18 shows the denoised results after implementing the proposed method ($m = 100$, $\lambda = 0.01$ in this case). It is seen that as expected, all the outliers have been effectively removed by HRPCA. It justifies again the capability of the proposed HRPCA method for outlier removal.

Under some special operational conditions or periods (including temporary malfunction of the data acquisition system and/or sensors), the acceleration response signals collected from the Canton Tower by the SHM system may contain densely corrupted outliers. Such an example is illustrated in Figure 1 in Section 1, which is a set of 19-h acceleration response data of the Canton Tower, collected at 00:00 to 19:00 on July 26, 2020 (Case 4). It is observed that large-amplitude spikes appear almost every 5 min in the time series of the acceleration data and shift the dynamic response deviating from zero mean. Such heavy contamination will definitely mask the true signal to a certain extent. After a careful check, it was found that the densely corrupted outliers were caused due to temporary malfunction of the data acquisition system in that period (the timing signal emitted every 5 min intervened with the acceleration response signal, resulting in outliers every 5 min).

To remove such anomalies and restore the true acceleration response data, we implement the proposed HRPCA method ($m = 100$, $\lambda = 0.005$ in this case) on the contaminated data. From the denoised results shown in Figure 19, it is seen that those anomalies appearing at intervals are favorably removed, and the true acceleration data are satisfactorily restored with its mean around zero. To sum up, the proposed HRPCA method is competent for outlier detection and identification and for fault data recovery.

5 | CONCLUSIONS

This study proposed a novel robust gross outlier removal method, named HRPCA, to effectively remove the unwanted gross outliers embedded in the monitoring data of structural dynamic responses and restore the true data. Based on the fundamental duality, the redundant yet relevant monitoring data are used to construct the low-rank Hankel matrix. After factorization by RPCA, the outliers are removed and the corrupted data is recovered.

The proposed method has been verified by an experimental study and using real-world SHM data acquired from a long-span bridge and a high-rise structure, where the performance of the proposed method was compared with that of four existing methods. The main conclusions are summarized as follows: (i) by comparing the performance metrics (i.e., SNR and PrmsD), the experiment shows that the proposed HRPCA method achieves better denoising performance than other four methods (the median filter, PCP, SVD, and wavelet), no matter whether the signal is stationary or non-stationary; (ii) the trade-off parameter λ can be determined by slightly tuning the value calculated from the universal selection criterion, and the annihilating length m can be set as a large value that satisfies the basic requirements ($m \geq k+1$ and $n-m+1 > k$) in practical applications; (iii) once it satisfies the basic requirements, the parameter m does not largely influence the denoising performance, and the optimal value of λ is not significantly affected by m; and (iv) the verification using real-world SHM data contaminated by varying degrees of outliers (single outlier, multiple outliers, and periodic and heavily polluted outliers) demonstrates the effectiveness of the proposed HRPCA method for outlier detection and removal and for fault data recovery under diverse outlier scenarios.

ACKNOWLEDGMENTS

The work described in this paper was supported by a grant from the Research Grants Council of the Hong Kong Special Administrative Region (SAR), China (Grant No. PolyU 152014/18E) and a grant from the National Natural Science Foundation of China (Grant No. U1934209). The authors also appreciate the funding support by the Innovation and Technology Commission of Hong Kong SAR Government to the Hong Kong Branch of Chinese National Rail Transit Electrification and Automation Engineering Technology Research Centre (Grant No. K-BBY1).

AUTHOR CONTRIBUTIONS

Si-Yi Chen: Conceptualization, methodology, formal analysis, software, writing – original draft. **You-Wu Wang:** Validation, supervision, writing – review & editing. **Yi-Qing Ni:** Conceptualization, supervision, resources, project administration, funding acquisition, writing – review & editing.

DATA AVAILABILITY STATEMENT

The data that support the findings of this study are available from the authors upon reasonable request.

REFERENCES

1. Cross EJ, Koo KY, Brownjohn JM, Worden K. Long-term monitoring and data analysis of the Tamar bridge. *Mech Syst Signal Process*. 2013;35(1–2):16-34. doi:10.1016/j.ymssp.2012.08.026
2. Wong KY. Design of a structural health monitoring system for long-span bridges. *Struct Infrastruct Eng*. 2007;3(2):169-185. doi:10.1080/15732470600591117
3. Ni YQ, Xia Y, Liao WY, Ko JM. Technology innovation in developing the structural health monitoring system for Guangzhou New TV Tower. *Struct Control Health Monit*. 2009;16(1):73-98. doi:10.1002/stc.303
4. Hu WH, Said S, Rohrmann RG, Cunha Á, Teng J. Continuous dynamic monitoring of a prestressed concrete bridge based on strain, inclination and crack measurements over a 14-year span. *Struct Health Monit*. 2018;17(5):1073-1094. doi:10.1177/1475921717735505
5. Fan W, Qiao P. Vibration-based damage identification methods: a review and comparative study. *Struct Health Monit*. 2011;10(1):83-111. doi:10.1177/1475921710365419
6. Nagarajaiah S, Erazo K. Structural monitoring and identification of civil infrastructure in the United States. *Struct Monit Maint*. 2016;3(1):51-69. doi:10.12989/smm.2016.3.1.051
7. Bao Y, Chen Z, Wei S, Xu Y, Tang Z, Li H. The state of the art of data science and engineering in structural health monitoring. *Engineering*. 2019;5(2):234-242. doi:10.1016/j.eng.2018.11.027
8. Fan G, Li J, Hao H. Vibration signal denoising for structural health monitoring by residual convolutional neural networks. *Measurement*. 2020;157:107651 doi:10.1016/j.measurement.2020.107651
9. Zhou C, Zhang Y. Particle filter based noise removal method for acoustic emission signals. *Mech Syst Signal Process*. 2012;28:63-77. doi:10.1016/j.ymssp.2011.08.004
10. Ahn D, Park J, Kim C, Kim J, Qian Y, Itoh T. A design of the low-pass filter using the novel microstrip defected ground structure. *IEEE Trans Microw Theory Tech*. 2001;49(1):86-93. doi:10.1109/22.899965
11. Jiang X, Mahadevan S, Adeli H. Bayesian wavelet packet denoising for structural system identification. *Struct Control Health Monit*. 2007;14(2):333-356. doi:10.1002/stc.161
12. Chegini SN, Bagheri A, Najafi F. Application of a new EWT-based denoising technique in bearing fault diagnosis. *Measurement*. 2019;144:275-297. doi:10.1016/j.measurement.2019.05.049
13. Yi TH, Li HN, Zhao XY. Noise smoothing for structural vibration test signals using an improved wavelet thresholding technique. *Sensors*. 2012;12(8):11205-11220. doi:10.3390/s120811205
14. Žvokelj M, Zupan S, Prebil I. Non-linear multivariate and multiscale monitoring and signal denoising strategy using kernel principal component analysis combined with ensemble empirical mode decomposition method. *Mech Syst Signal Process*. 2011;25(7):2631-2653. doi:10.1016/j.ymssp.2011.03.002
15. Golafshan R, Yuce Sanliturk K. SVD and Hankel matrix based de-noising approach for ball bearing fault detection and its assessment using artificial faults. *Mech Syst Signal Process*. 2016;70:36-50. doi:10.1016/j.ymssp.2015.08.012
16. Yang Y, Rao J. Robust and efficient harmonics denoising in large dataset based on random SVD and soft thresholding. *IEEE Access*. 2019;7:77607-77617. doi:10.1109/ACCESS.2019.2921579
17. Zhao M, Jia X. A novel strategy for signal denoising using reweighted SVD and its applications to weak fault feature enhancement of rotating machinery. *Mech Syst Signal Process*. 2017;94:129-147. doi:10.1016/j.ymssp.2017.02.036
18. Ke L. Denoising GPS-based structure monitoring data using hybrid EMD and wavelet packet. *Math Probl Eng*. 2017;2017:4920809 doi:10.1155/2017/4920809
19. Miao F, Zhao R, Wang X. A new method of denoising of vibration signal and its application. *Shock Vib*. 2020;2020:7587840 doi:10.1155/2020/7587840
20. Worden K, Dulieu-Barton JM. An overview of intelligent fault detection in systems and structures. *Struct Health Monit*. 2004;3(1):85-98. doi:10.1177/1475921704041866
21. Bao Y, Tang Z, Li H, Zhang Y. Computer vision and deep learning-based data anomaly detection method for structural health monitoring. *Struct Health Monit*. 2019;18(2):401-421. doi:10.1177/1475921718757405
22. Tang Z, Chen Z, Bao Y, Li H. Convolutional neural network-based data anomaly detection method using multiple information for structural health monitoring. *Struct Control Health Monit*. 2019;26(1):e2296 doi:10.1002/stc.2296
23. Fu Y, Peng C, Gomez F, Narazaki Y, Spencer BF Jr. Sensor fault management techniques for wireless smart sensor networks in structural health monitoring. *Struct Control Health Monit*. 2019;26(7):e2362 doi:10.1002/stc.2362
24. Arul M, Kareem A. Data anomaly detection for structural health monitoring of bridges using shapelet transform. arXiv preprint arXiv:2009.00470. 2020 31.
25. Mao J, Wang H, Spencer BF Jr. Toward data anomaly detection for automated structural health monitoring: exploiting generative adversarial nets and autoencoders. *Struct Health Monit*. 2021;20(4):1609-1626. doi:10.1177/1475921720924601
26. Pimentel MA, Clifton DA, Clifton L, Tarassenko L. A review of novelty detection. *Signal Process*. 2014;99:215-249. doi:10.1016/j.sigpro.2013.12.026
27. Chandola V, Banerjee A, Kumar V. Anomaly detection: a survey. *ACM Comput Surv*. 2009;41(3):1-58. doi:10.1145/1541880.1541882

28. Yang Y, Nagarajaiah S. Blind denoising of structural vibration responses with outliers via principal component pursuit. *Struct Control Health Monit*. 2014;21(6):962-978. doi:10.1002/stc.1624
29. Jin KH, Lee D, Ye JC. A general framework for compressed sensing and parallel MRI using annihilating filter based low-rank Hankel matrix. *IEEE Trans Computat Imag*. 2016;2(4):480-495. doi:10.1109/TCI.2016.2601296
30. Lee J, Jin KH, Ye JC. Reference-free single-pass EPI Nyquist ghost correction using annihilating filter-based low rank Hankel matrix (ALOHA). *Magn Reson Med*. 2016;76(6):1775-1789. doi:10.1002/mrm.26077
31. Lee D, Jin KH, Kim EY, Park SH, Ye JC. Acceleration of MR parameter mapping using annihilating filter-based low rank Hankel matrix (ALOHA). *Magn Reson Med*. 2016;76(6):1848-1864. doi:10.1002/mrm.26081
32. Hu Y, Liu X, Jacob M. A generalized structured low-rank matrix completion algorithm for MR image recovery. *IEEE Trans Med Imag*. 2018;38(8):1841-1851. doi:10.1109/TMI.2018.2886290
33. Jin KH, Ye JC. Sparse and low-rank decomposition of a Hankel structured matrix for impulse noise removal. *IEEE Trans Image Process*. 2017;27(3):1448-1461.
34. Jin KH, Um JY, Lee D, Lee J, Park SH, Ye JC. MRI artifact correction using sparse + low-rank decomposition of annihilating filter-based hankel matrix. *Magn Reson Med*. 2017;78(1):327-340. doi:10.1002/mrm.26330
35. Ye JC, Kim JM, Jin KH, Lee K. Compressive sampling using annihilating filter-based low-rank interpolation. *IEEE Trans Inf Theor*. 2016;63(2):777-801.
36. Kim TH, Bilgic B, Polak D, Setsompop K, Haldar JP. Wave-LORAKS: combining wave encoding with structured low-rank matrix modeling for more highly accelerated 3D imaging. *Magn Reson Med*. 2019;81(3):1620-1633. doi:10.1002/mrm.27511
37. Ongie G, Jacob M. Off-the-grid recovery of piecewise constant images from few fourier samples. *SIAM J Imag Sci*. 2016;9(3):1004-1041. doi:10.1137/15M1042280
38. Vetterli M, Marziliano P, Blu T. Sampling signals with finite rate of innovation. *IEEE Trans Signal Process*. 2002;50(6):1417-1428. doi:10.1109/TSP.2002.1003065
39. Maravic I, Vetterli M. Sampling and reconstruction of signals with finite rate of innovation in the presence of noise. *IEEE Trans Signal Process*. 2005;53(8):2788-2805. doi:10.1109/TSP.2005.850321
40. Candès EJ, Li X, Ma Y, Wright J. Robust principal component analysis? *J ACM*. 2011;58(3):1-37. doi:10.1145/1970392.1970395
41. Chandrasekaran V, Sanghavi S, Parrilo PA, Willsky AS. Rank-sparsity incoherence for matrix decomposition. *SIAM J Optim*. 2011;21(2):572-596. doi:10.1137/090761793
42. Ying ZG, Wang YW, Ni YQ, Xu C. Model-free identification of multiple periodic excitations and detection of structural anomaly using noisy response measurements. *Smart Struct Syst*. 2021;28(3):407-423.
43. Middleton D. Statistical-physical models of electromagnetic interference. *IEEE Trans Electromagn Compat*. 1977;3(3):106-127. doi:10.1109/TEMC.1977.303527
44. Bhatti SA, Shan Q, Glover IA, et al. Impulsive noise modelling and prediction of its impact on the performance of WLAN receiver. In: *Proceeding of 17th European signal processing conference*. Glasgow, Scotland; 2009:1680-1684.
45. Ravizza G, Ferrari R, Rizzi E, Dertimanis V, Chatzi EN. Denoising corrupted structural vibration response: critical comparison and assessment of related methods. In: *Proceeding of 7th international conference on computational methods in structural dynamics and earthquake engineering*. Crete, Greece; 2019:3893-3904.
46. Costabel S, Müller-Petke M. Despiking of magnetic resonance signals in time and wavelet domains. *Near Surface Geophys*. 2014;12(2):185-198. doi:10.3997/1873-0604.2013027
47. Loizou PC. *Speech enhancement: Theory and practice*. 2nd ed. New York, USA: CRC Press; 2013.
48. Ni YQ, Wong KY, Xia Y. Health checks through landmark bridges to sky-high structures. *Adv Struct Eng*. 2011;14(1):103-119. doi:10.1260/1369-4332.14.1.103
49. Ni YQ, Wang YW, Liao WY, Chen WH. A vision-based system for long-distance remote monitoring of dynamic displacement: experimental verification on a supertall structure. *Smart Struct Syst*. 2019;24(6):769-781.
50. Wang YW, Ni YQ. Full-scale monitoring of wind effects on a supertall structure during six tropical cyclones. *J Build Eng*. 2022;45:103507 doi:10.1016/j.jobe.2021.103507

How to cite this article: Chen S-Y, Wang Y-W, Ni Y-Q. Gross outlier removal and fault data recovery for SHM data of dynamic responses by an annihilating filter-based Hankel-structured robust PCA method. *Struct Control Health Monit*. 2022;29(12):e3144. doi:10.1002/stc.3144